AGU PUBLICATIONS

JGR

Journal of Geophysical Research: Oceans

RESEARCH ARTICLE

10.1002/2016JC011729

Behavior of a wave-driven buoyant surface jet on a coral reef

Liv M. M. Herdman[1], James L. Hench[2], Oliver Fringer[1], and Stephen G. Monismith[1]

[1]Environmental Fluid Mechanics Laboratory, Stanford University, Stanford, California, USA, [2]Duke University Marine Laboratory, Nicholas School of the Environment, Beaufort, North Carolina, USA

Key Points:
- Reef-ocean temperature gradients are important in regulating reef-ocean exchange
- Substantial recirculation of wave-driven jets exiting reef passes can occur
- Alongshore velocity is important in determining amount of jet recirculation

Correspondence to:
L. M. M. Herdman,
lherdman@usgs.gov

Citation:
Herdman, L. M. M., J. L. Hench, O. Fringer, and S. G. Monismith (2017), Behavior of a wave-driven buoyant surface jet on a coral reef, *J. Geophys. Res. Oceans*, *122*, 4088–4109, doi:10.1002/2016JC011729.

Received 15 FEB 2016
Accepted 28 FEB 2017
Accepted article online 7 MAR 2017
Published online 16 MAY 2017

Abstract A wave-driven surface-buoyant jet exiting a coral reef was studied in order to quantify the amount of water reentrained over the reef crest. Both moored observations and Lagrangian drifters were used to study the fate of the buoyant jet. To investigate in detail the effects of buoyancy and alongshore flow variations, we developed an idealized numerical model of the system. Consistent with previous work, the ratio of alongshore velocity to jet velocity and the jet internal Froude number were found to be important determinants of the fate of the jet. In the absence of buoyancy, the entrainment of fluid at the reef crest creates a significant amount of retention, keeping 60% of water in the reef system. However, when the jet is lighter than the ambient ocean water, the net effect of buoyancy is to enhance the separation of the jet from shore, leading to a greater export of reef water. Matching observations, our modeling predicts that buoyancy limits retention to 30% of the jet flow for conditions existing on the Moorea reef. Overall, the combination of observations and modeling we present here shows that reef-ocean temperature gradients can play an important role in reef-ocean exchanges.

1. Introduction

Ocean-lagoon exchange plays a key role in setting water residence time in coral reef lagoons, thus affecting nutrient concentrations [*Charpy*, 2001], carbon system dynamics [*Falter et al*., 2013], temperature (and thus thermal stresses) [*Zhang et al*., 2013; *Davis et al*., 2011], and sediment concentrations [*Golbuu et al*., 2003]. Fluxes of new ocean water entering reef lagoons have also been found to be important in controlling the supply of plankton to inshore reefs [*Wyatt et al*., 2010]. Conversely, it is likely that export of plankton and larvae to other nearby reef systems or equivalently, the retention of plankton and larvae in a given system, will be controlled by the ocean-lagoon exchange. Thus, hydrodynamic processes that drive variability of ocean-lagoon exchange in coral reef systems are likely to drive concomitant variability in biogeochemical and ecological functioning of these systems.

Circulation in many reef systems is dominated by surface waves, which break on the steep slopes of the reef and drive a flux of water over the reef crest [*Hearn*, 1999; *Gourlay and Colleter*, 2005; *Callaghan et al*., 2006; *Hench et al*., 2008]. The water entering over the reef crest then returns to the ocean through reef passes, i.e., gaps in the reef, as a jet driven by the pressure gradients created by the waves. The size and shape of these reef pass systems play an important role in predicting exchange. *Lowe et al*. [2009a] found that the reef geometry and roughness determined flow and thus residence times because the amount of friction along the flow path changed the dynamics in the back reef. *Monismith* [2014] also found that the shape of the lagoon and amount of friction is important to determine the path of flow exiting the pass.

Extensive study of inlets has been performed in tidally driven inlet exchanges particularly in the estuarine environment [*Stommel and Farmer*, 1952; *Hench and Luettich*, 2003]. It has been found that the asymmetry between the ebb-jet and flood-sink creates a residual flow at the inlet that determines net exchange. The pattern of recirculation and exchange in tidally pumped inlets is controlled by the width of the inlet and spatial variability in tidal phase, as the primary factors controlling tidal asymmetry [*Stommel and Farmer*, 1952; *Chant*, 2011]. Here, given the limited role of tides, we expect to find a very different spatial pattern of exchange, however, for a given flow, the width of the inlet may still be important. The amount of exchange at an inlet can be defined by a tidal exchange ratio, that is the percent of new water entering on a tidal cycle relative to the total amount of water entering through the inlet [*Fischer et al*., 1979]. The strength of the alongshore flow is an important factor in predicting this ratio and it has also been identified in

predicting ocean exchange with reefs and small embayments[*Black et al.*, 1990; *Sanford et al.*, 1992]. Strong, steady, alongshore currents can advect away reef and lagoon water in the pass jet and greatly reduce retention, while weak unsteady currents may increase residence times [*Black et al.*, 1990].

In the wave-driven reef pass case, the amount of exchange is not driven by a tidal asymmetry, as the jet exiting through the pass (although unsteady) does not reverse direction periodically and is usually unidirectional (Figure 1). However, the geometry of a system, with wave-driven inflow opposing the direction of the jet creates the possibility of significant retention of outflowing water. To our knowledge, the mechanisms controlling retention of water exiting through reef-passes as wave-driven jets has not been previously examined, despite this being a common geometry and exchange mechanism in coral reefs.

The water exiting a reef pass is a special case of a surface-buoyant jet in the coastal environment. Many studies have explored surface-buoyant discharges [e.g., *McGuirk and Rodi*, 1978; *Baddour and Chu*, 1986; *Nash and Jirka*, 1996; *Horner-Devine*, 2009; *Chant*, 2011]; while this work is applicable to the wave-driven jet, the additional factor of the jet exiting adjacent to a reef crest that is entraining fluid must also be considered. From this work, three nondimensional parameters are identified as important in describing the dynamics [*Jirka*, 2004; *Jones et al.*, 2007; *Fischer et al.*, 1979]. They are the internal Froude Number of the jet (F_{jet})

$$F_{jet} = U_{jet}/\sqrt{g'h}, \tag{1}$$

is the shape factor (S) representing the ratio of the jet width (b) to the depth (h) at the opening

$$S = b/h, \tag{2}$$

and the velocity ratio

$$R = U_a/U_{jet} \tag{3}$$

where U_{jet} is the velocity of the jet at the opening and g' is gravity modified by the buoyancy difference between the jet and ambient ocean water such that $g' = g(\rho_j - \rho_o)/\rho_o$. The internal Froude number (F_{jet}) compares the relative importance of the initial jet momentum to the initial jet buoyancy. The shape factor (S) can be thought of in terms of the effect of bottom friction on the jet. The wider and shallower the jet, i.e., the higher S is, the more important friction will be in the dynamics. The velocity ratio is the ratio of the alongshore velocity to the initial jet velocity, which compares the relative strengths of momentum of the jet and the alongshore flow. In larger passes or rivers Coriolis may be important, but in this situation the Coriolis force is not dynamically important, with a Rossby number (Ro = U/fL) of 15 for a jet with 10 cm/s exit speed, a width of 300 m, and an inertial frequency of 2.2×10^{-5} rad/s.

The strength of the alongshore flow relative to the jet is critical for predicting shoreline reattachment. In the case of a fringing reef system, the shoreline is replaced by an open reef crest, so the conditions that would

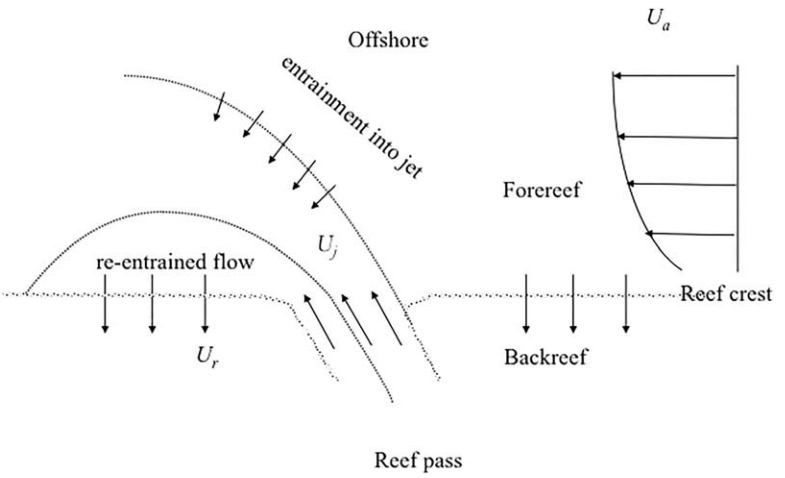

Figure 1. Schematic of a wave-driven jet exiting a reef pass with alongshore flow.

equate reattachment in a beach case will actually cause a recirculation of jet fluid back over the reef crest. Thus, to predict the net exchange, we must understand what conditions cause the jet to attach to the "shore." The alongshore flow adds momentum to the jet, via entrainment, and can also create a pressure form-drag force as it flows around the jet [*Jirka*, 2007]. Both effects cause the jet to deflect in the direction of the cross flow. *Chu and Abdelwahed* [1990] found that the best parameter for predicting shoreline reattachment of a buoyant jet in an unconfined flow is the composite Froude number of $F_{jet}F_a$ where F_{jet} is the jet internal Froude number defined earlier, and F_a is the Froude number for the ambient flow and uses the alongshore velocity instead of the jet velocity. They found that downstream attachment does not occur for $F_{jet}F_a > 0.5$. This indicates that to produce a strongly curving jet, momentum either alongshore or within the jet needs to be strong relative to the buoyancy forcing.

The goal of this work is to understand what factors are important in predicting the net export of water from the reef in a jet exiting a reef pass, or equivalently the fraction of flow that is reentrained. Toward this end, we first describe the field site and the measurement techniques used to observe the fate of a wave-driven buoyant jet exiting a reef pass. The resulting observations are used to motivate the modeling work that follows. In the second section, we describe the idealized numerical model used and show the effects of systematically varying buoyancy and alongshore flow on the fate of the jet. Finally, we discuss the net effect of the reef crest on the recirculation of the jet and share our conclusions.

2. Observations

2.1. Field Site

The study site was the reef and lagoon system on the north shore of Moorea (17° 28.9′ S; 149° 50.3′ W) described by *Hench et al*. [2008]. It has a well-developed fringing reef and lagoon system. There are four main parts to the reef, each with different physical and biological characteristics; the fore-reef, the back reef and reef crest, the bay, and the reef pass (Avaroa Pass) that connects the back reef and lagoon to the ocean. These locations are labeled on a bathymetric plot of the study area in Figure 2. This work is primarily concerned with what occurs offshore of the reef crest and the water emanating from the pass. Offshore of the fore-reef the bottom slope averages 1:8 although there is smaller-scale spur and groove structure between 0 and 30 m in depth. Offshore and deeper than the spur and grove structure the bottom was predominantly sandy. Waves approaching the north shore break as the reef shallows, creating coral rubble and leaving little live coral in the surf zone.

The reef crest is the shallowest point and during low wave conditions is covered by 10–20 cm of water. However, with the large waves that are prevalent in austral summer the water-level can increase by up to 0.5 m due to wave breaking and wave-setup leading to water depths up to 1 m [*Monismith et al*., 2013]. Avaroa Pass lies directly north of the bay, connecting the reef and lagoon system to the ocean. The pass is about 300 m wide and has a maximum depth of 50 m in a scour hole, although most of the pass is 30 m deep. The bottom of the pass is covered in sand and coral rubble. The sides of the pass rise steeply to the shallow back-reef with a slope of about 1:3. While the reef crest runs almost due east-west, the reef pass is aligned approximately 15° west of north.

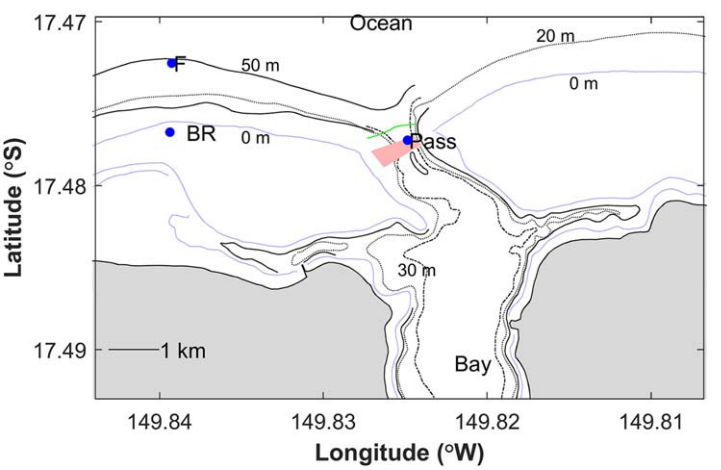

Figure 2. Bathymetry of field site with mooring locations. The mooring locations referred to in the text are indicated with blue dots. Green line indicates location of ADCP transect (shown in Figure 6) and drifter release area is shown with red shading.

2.2. Observational Methods

We carried out two field experiments, one from December 2006 to February 2007 and the second between December 2008 and February 2009. During

these experiments, we used a combination of moored ADPs, CTDs, and temperature probes, shipboard ADCP/CTD transects, as well as radio-tracked GPS drifters. The data presented in this paper include information from two ADCPs, one placed within the center of the pass (Pass Station in Figure 2) to the ocean at 43 m depth, and one placed on the fore-reef at 40 m water depth (Station F in Figure 2). Colocated with the reef pass ADCP was a string of CTDs deployed at 6, 10, 21, 26, and 43 m depths. ADP and temperature logger were located just behind the reef crest (Station *R* in Figure 2) in 2 m of water.

Velocity sections were also measured across the mouth of the pass with vessel-mounted 300 kHz and 1.2 MHz ADCPs to simultaneously resolve near surface and deep-water velocities, which recorded single ping data at 1.66 Hz in 4 m bins and 5 Hz in 0.5 m bins, respectively. The vessel position was determined with a Trimble Geo Explorer GPS such that in conjunction with a base station located on land, postprocessing of the GPS data yielded an error in position of less than 0.5 m.

The drifters we released were built to survive the surf-zone, where wave breaking can exert strong forces on the drifters, and not get caught in the shallow back reef, where coral bommies regularly reach within centimeters of the surface. Our design was based on the surf zone drifter in *Johnson and Pattiaratchi* [2004], but with several modifications to facilitate easier deployment in a shallow coral reef environment. Our drifter extended to a water depth of 0.5 m and the PVC housing that held the GPS drifter was 20 cm long with the top 5 cm reaching above the water. The righting moment of the drifter was maintained with a 4 cm section of closed-cell floatation foam around the PVC housing and a 30 g lead weight sewn into the bottom of a single 0.3 m long parachute drogue. The performance of these drifters was tested for wind slip and wave surfing against more standard Davis-style (and other) drifter designs and had very similar trajectories [*Herdman*, 2012]. Individual drifter positions were determined using GPS receiver unit (Garmin RINO 520) which recorded drifter positions at 0.25 Hz. Tests of the accuracy of the GPS units [*Herdman*, 2012] indicate that the error in position would produce errors in the drifter velocities much smaller than those anticipated from wind slip. Wind slip has been found to be up to half a percent of the wind speed [*Niiler and Paduan*, 1995; *Johnson et al*., 2003] with average wind speeds in Moorea generally below 5 ms^{-1} [*Herdman et al*., 2015] the error in drifter velocities can be up to 2.5 cms^{-1}.

2.3. Observations: Flow Near the Reef Pass (the Jet Source)

During the austral summer the net flow from the pass was always out, i.e., from the reef to the ocean. The flow leaving the pass typically was separated from the bottom at the location of our mooring but at times the jet remained bottom attached (Figures 3 and 4). Given that the source of this flow is supplied by the wave-driven flow over the reef crest [*Hench et al*., 2008; *Herdman et al*., 2015], the strength of wave forcing determines when the outflow extends over the entire depth near the mouth of the pass. The volume flux varied between 0 and 3100 m^3s^{-1} during the time period shown, with an average of 1100 m^3s^{-1} (Figure 4a). Velocity in the lower layer varied from 0 to -0.4 ms^{-1} (negative meaning inflow into the pass). Even when the net flux was zero, the surface jet had not stopped flowing; instead, the flow in the surface jet out of the pass was balanced by the inwards flow of ocean water in the lower layer [see *Hench et al*., 2008]. The density difference between the two layers ranged from 2.3×10^{-2} kg m^{-3} to 2 kg m^{-3} with the average density difference of $\sim$0.5 kg m^{-3} (Figure 4b). With the exception of a large flood event in the week of 14 January, this density difference was primarily due to differences in temperature. During the time period of data collection, the alongshore velocity ranged from -0.36 to 0.42 m/s, creating a velocity ratio that ranged from zero to 7. (Figure 4d).

2.4. Drifter Trajectories

In order to follow the fate of the jet water, drifters were released across the mouth of the pass spaced about 100 m apart. Each release consisted of 5–20 drifters and lasted between 0.5 and 5 h. Each line was 5 or 6 drifters long and a new line was released every 20 min until there were no more drifters, resulting in 2–4 lines across the pass per release. The details of each release are shown in Table 1.

The trajectories for all of the pass releases are shown in Figure 5. In these different realizations, we observe the variability of the fate of the surface water exiting the pass. In most releases, we observed a high percentage of drifters become entrained in the offshore flow and get transported away from the lagoon system. The remaining fraction of water that exits the pass is reentrained into the wave-driven flow and recirculated

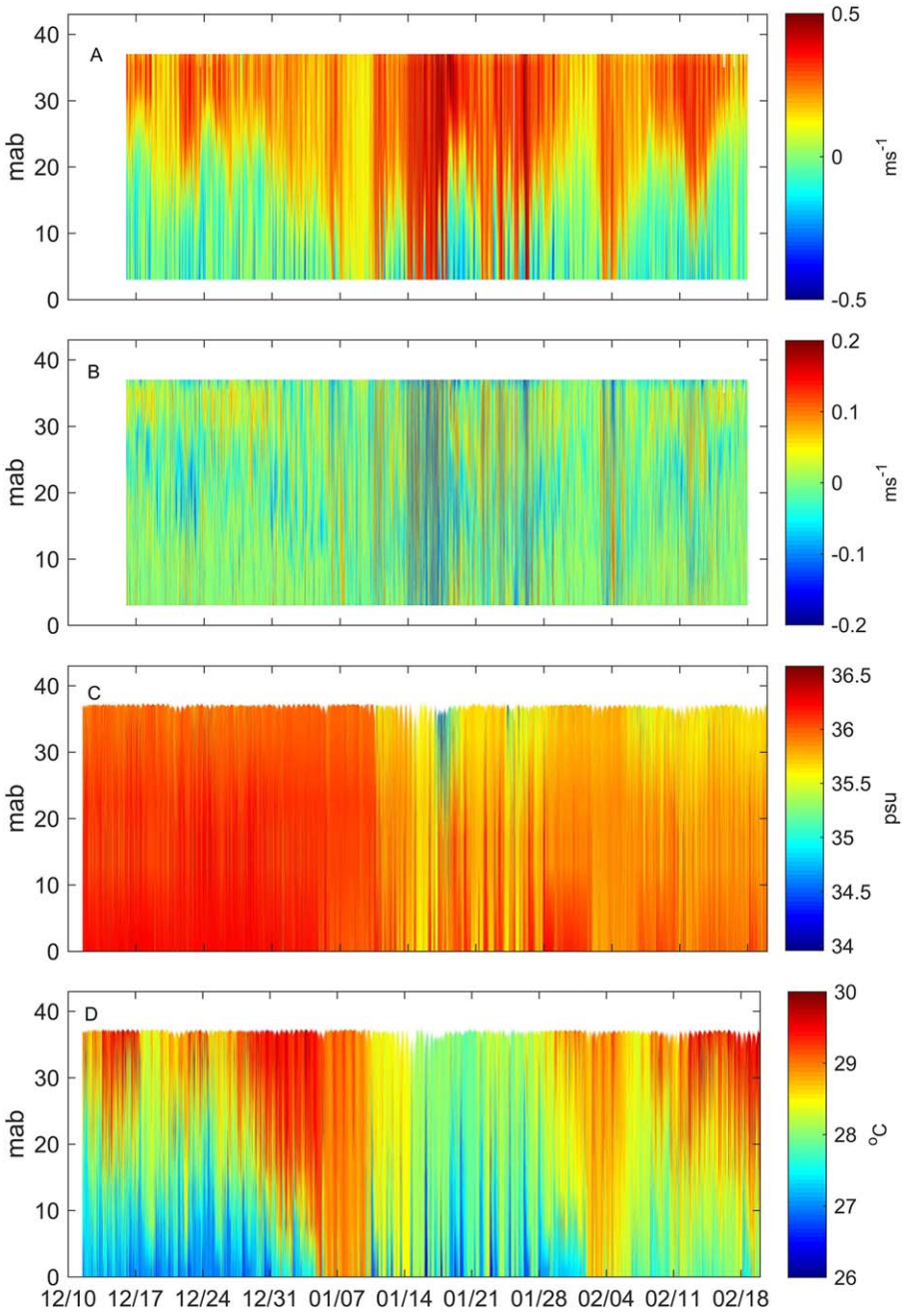

Figure 3. Jet initial conditions measured over the austral summer December 2006 to February 2007: (a) The along pass velocity positive toward the ocean. (b) Across pass velocity (positive to the west). (c) Salinity and (d) temperature.

through the system. In our 16 releases, we observe the two extremes of almost total reentrainment (Figures 5g and 5o) and no reentrainment (Figure 5f).

In Figure 5o, the drifters split and return over the reef crest on both the east and west sides of the pass. The east channel more directly fed the pass while the drifters coming through the west back reef headed to the bay before [see *Herdman et al.*, 2015] eventually exiting through the pass. Only one drifter headed offshore and thus away from the reef. In Figure 5g, the drifters are seen to immediately head over the west reef crest after leaving the pass. In Figure 5f, the jet appears to be extremely strong with the drifters traveling at speeds of 70 cms^{-1} and going 1 km or more offshore before being entrained into the alongshore current.

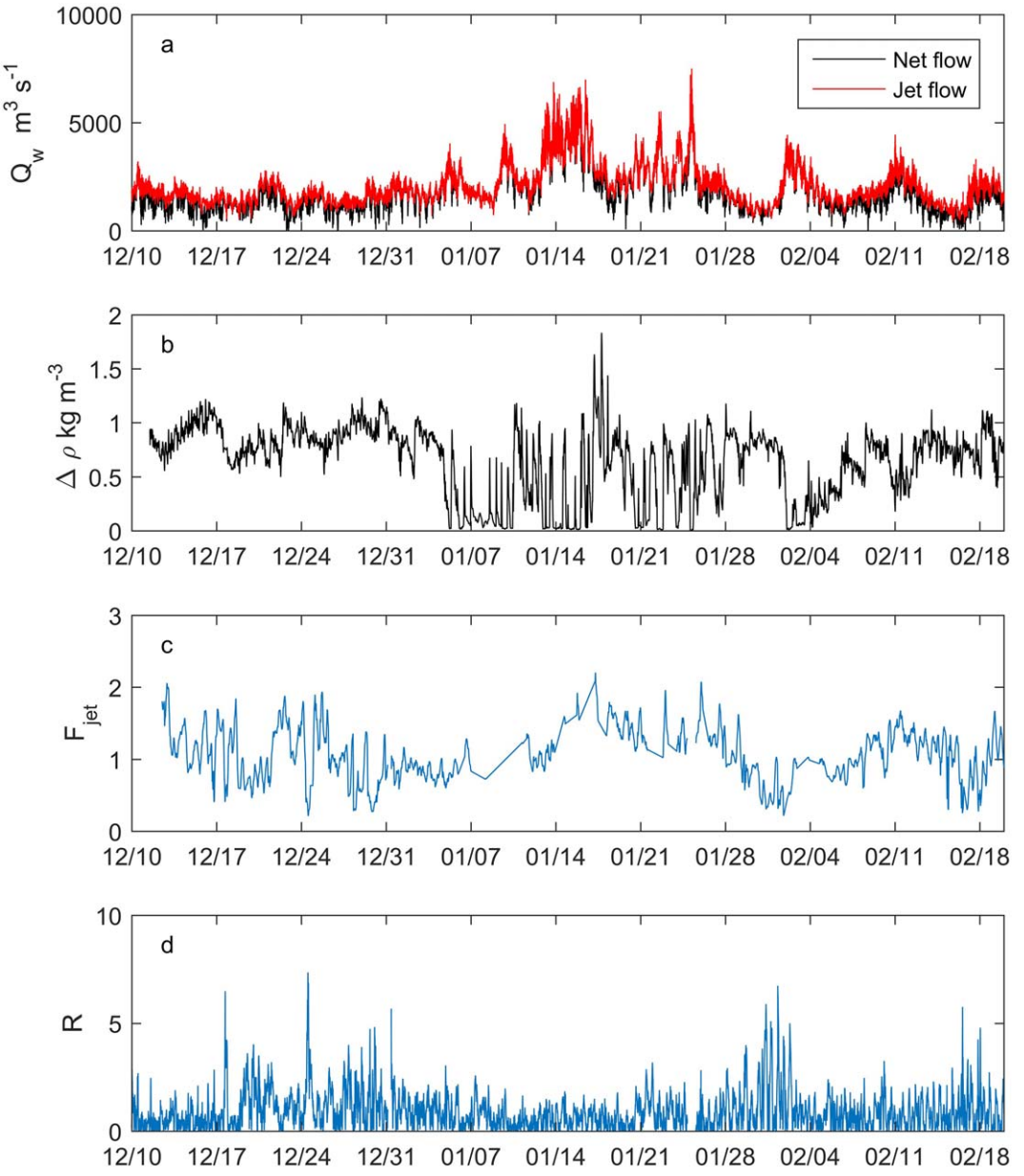

Figure 4. Jet initial conditions measured over the austral summer December 2006 to February 2007: (a) The net ocean ward flow and the flow out of the jet. (b) Top bottom density difference, (c) Jet Froude number, (d) velocity ratio, *R*, of alongshore to jet velocity.

Once the drifters leave the pass and enter the fore-reef, they begin to "feel" the wave-driven cross-shore flow. While being carried steadily by the alongshore current, they simultaneously were pushed toward the reef crest by the wave-driven flow over the reef crest. The curvature of the streamlines seen in Figure 5 is due to two factors: (1) lateral shear in the alongshore current, evidently the result of the frictional coastal boundary layer on the fore-reef; and (2) the fact that the mean Lagrangian velocity of the cross-shore flow varies inversely with depth means that the drifters will accelerate as they approach the reef crest [cf., *Monismith et al.*, 2013]. Once they passed over the reef crest onto the back reef, they decelerated in the deeper water of the reef flat, eventually traveling to the channels that feed Avaroa Pass.

2.5. Estimates of Retention From Observations

The fraction of retention of jet water was highly variable, depending on the conditions during each drifter release. In the following section, we investigate the spatial patterns in average recirculation, the effect of alongshore flow strength, and the jet buoyancy on the recirculation. Figure 6a shows the spatial variability

Table 1. GPS Drifter Release Times and Deplement Durations[a]

Release	Date	Num. Drifters	Duration (min)
1	02/13/2007	10	20
2	02/14/2007	10	83
3	02/17/2007	8	62
4	02/18/2007	9	75
5	02/18/2007	10	300
6	02/19/2007	9	67
7	02/19/2007	9	67
8	12/09/2008	5	60
9	12/10/2008	20	220
10	12/10/2008	10	90
11	12/11/2008	20	210
12	02/11/2009	17	125
13	02/11/2009	16	200
14	02/12/2009	18	150
15	02/12/2009	18	250
16	02/13/2009	18	130
17	02/13/2009	16	160

[a]All sets of drifters were released along a transect across the reef pass.

in the retention fraction measured for the 16 drifter releases from the pass calculated as follows: the reef and near-shore area were divided into a grid of 10 m squares. The percentage of retention for each grid cell was determined by the number of drifters that passed through that cell that also eventually became entrained in offshore fluid and left the domain (or appeared that they would leave) relative to the total number of drifters that passed through that cell.

Retention is strongest near the edges of the pass, and is particularly strong on the west edge of the pass (Figure 6a). Across the entire mouth of the pass, there is no region from which particles (drifters) would always escape offshore from the reef system. It should be noted that these releases were all done during the winter time when the wave-driven flow over the reef was strong. Given that the back reef flow varies considerably with the seasons [*Hench et al*., 2008; *Herdman*, 2012], the recirculation pattern may also vary seasonally. The axis of the pass opening is oriented at about 30° west of north, i.e., not directly north and thus the fore-reef bathymetry changes the outflow jet's trajectory. Finally, because of the jet's initial velocity to the west, retention is stronger on the western side of the reef than if the jet exited perpendicularly to the reef crest. Reflecting the strength of the wave-driven flow on the fore-reef, on both sides of the jet it appears that if a drifter gets close enough to the reef crest, it is entrained into the flow over the reef crest.

In order to evaluate the dependence of recirculation on buoyancy, in Figures 6b and 6c we have done a similar calculation as in Figure 6a but have only included drifter runs based on internal Froude number condition. Froude numbers below 0.5 are considered low and Froude numbers above 1 are considered high. When buoyancy is the dominant force over momentum, we expect more symmetric entrainment patterns since buoyancy-driven flows will tend to spread radially, i.e., to the sides as much as offshore. This is clear in the low Froude number cases shown in Figure 6b. As a consequence, there is a greater rate of retention on the jet edge in these cases, and that high retention is seen on both sides of the pass. In the momentum-dominated cases (Figure 6c), the spatial pattern of retention reflects the orientation of the jet opening toward the west, which enhances retention on the west side of the reef, since the jet passes closer to the western reef crest. Because of the temporal variability of the alongshore flow, we were not able to examine how retention varied with the ratio of alongshore velocity to jet velocity ratios.

Practically, to define the effect of jet behavior on residence time, it is necessary to weight these retention statistics by fraction of outflow found at each lateral position in the pass. For example, the retention zones on the west side of the pass do not contribute as much to the return flow as do those on the east side of the pass. It is shallower so has less mass flux per unit width. With velocity measured in an ADCP transect across the pass, we can estimate the distribution of water exiting the pass (Figure 7b). The flow is relatively evenly distributed with a peak in water flux at 100 m from the western edge of the channel. The smaller fluxes at the edges can be attributed primarily to the depth of the pass. Also, due to bathymetry, the waves wrap around the reef on the western edge of the pass and directly oppose the jet, slowing the exit velocity.

We can combine the spatial variability of flux across the pass with the spatial variability of the retention (Figure 7a) to compute volume percentages of retention. For each 15 m width of the pass, we used the drifter data to estimate the probability that the water particles from that segment would permanently exit the reef lagoon system. Weighting this spatially variable retention rate by flow through that segment provides an estimate the total percentage of jet fluid that is retained by the system. Doing so for the average case, i.e., including all the drifter results, gives a net retention rate of about 33%. While segregation of the drifter releases by conditions based on Froude number or alongshore flow suggested retention rates between 23 and 50%, given a bootstrapped-derived estimated uncertainty in retention of ∼15%, these values were not

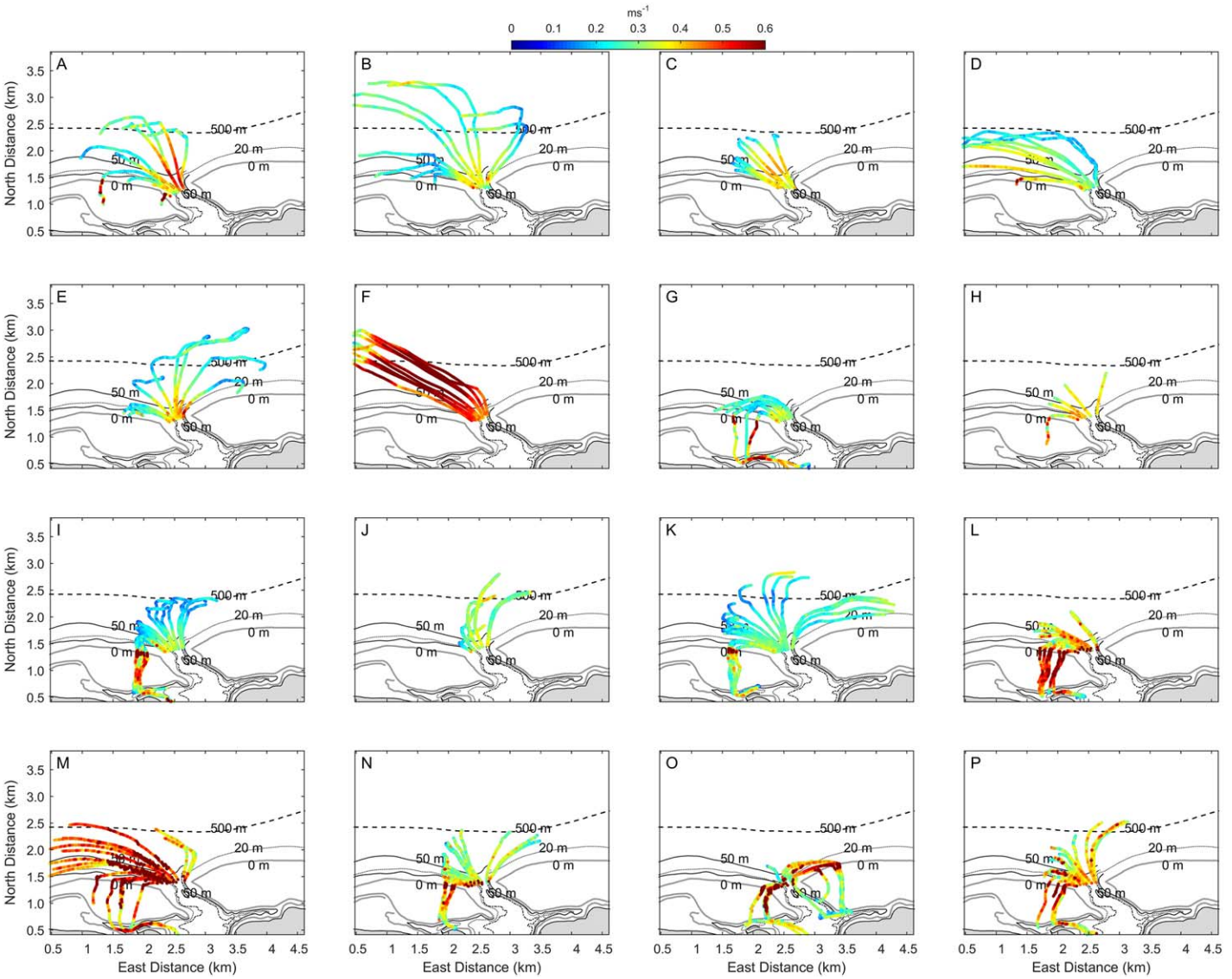

Figure 5. Drifter releases (1–16 in Table 1). Each point is a GPS position recorded with color indicating speed from 0 to 0.6 m/s as indicated by the color bar. X and Y axes in kilometers from an arbitrary zero.

statistically different from the average value. Nonetheless, the drifter data make clear spatial patterns in retention and even in the least retentive conditions, at least 20% of the water is retained by the system.

3. Numerical Modeling

3.1. Model Motivation and Design

Despite conducting 228 sets of drifter releases involving 68 h of drifter trajectory data, and, while broad patterns and rate of retention are discernable from our observations, we were not able to clearly separate out the different effects of the offshore current and the buoyancy on retention. To further pursue these, we carried out a modeling study using simplified bathymetry where we were able to control the alongshore velocity, jet momentum, buoyancy, and reef geometry.

To simplify the computations, rather than explicitly model the entire lagoon/reef system including explicit phase-averaged wave dynamics [as in *Lowe et al.*, 2009b], we chose to model the wave-driven flow by a sink/source combination distributed along one open boundary. The sink corresponds to the reef crest region, which entrains water from offshore and the source is chosen to represent the pass outflow. As

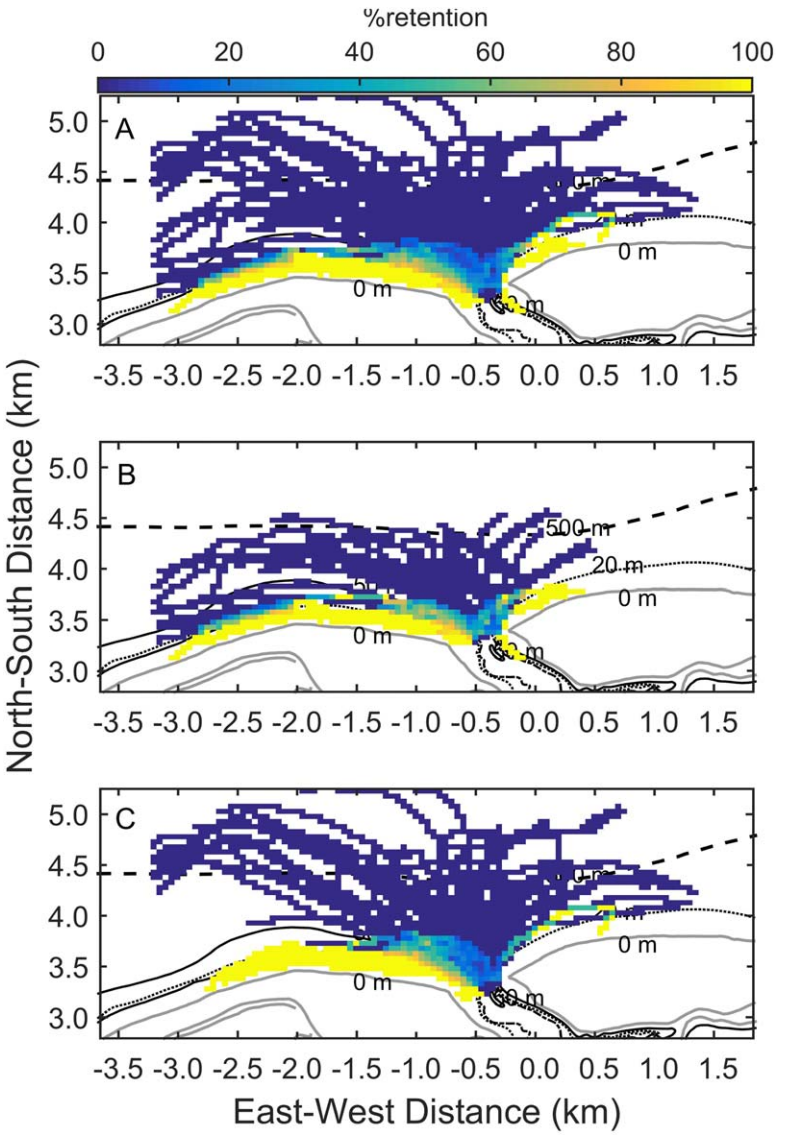

Figure 6. Spatial patterns of retention varying with F_{jet}: (a) average retention including all conditions; (b) Average retention for $F_{jet} < 1$(7 releases); and, (c) average retention for $F_{jet} > 1$ (10 releases). In each plot, the color indicates the percent chance of returning over the reef crest if a drifter passes through that cell.

described in more detail below, the total flow through the pass was set equal to the flow over the reef crest. The strength of the source/sink was chosen to model conditions observed on the Moorea reef [cf., *Monismith et al*., 2013].

3.2. Numerical Modeling Methods

We used the three-dimensional, unstructured-grid, finite-volume SUNTANS model [*Fringer et al*., 2006]. SUNTANS employs a semiimplicit free surface [*Casulli and Walters*, 2000] and computes the nonhydrostatic pressure, although in this paper we use the hydrostatic version. Temperature is advected with a higher-order flux-limiting scheme following *Casulli and Zanolli* [2005]. No diffusion is imposed for scalar transport, while a constant horizontal eddy-viscosity of $\nu_H = 0.1\ m^2\ s^{-1}$ is employed to stabilize central differencing of momentum advection. In the vertical, the *Mellor and Yamada* [1982] level 2.5 turbulence closure scheme is employed with stability functions modified by *Galperin et al*. [1988], and with a background eddy-viscosity of $\nu_V = 10^{-6}\ m^2\ s^{-1}$.

A triangular, unstructured grid was generated with GAMBIT (ANSYS Fluent). The alongshore velocity was imposed on the eastern boundary and the depth was fixed on the western boundary (Figure 8), allowing

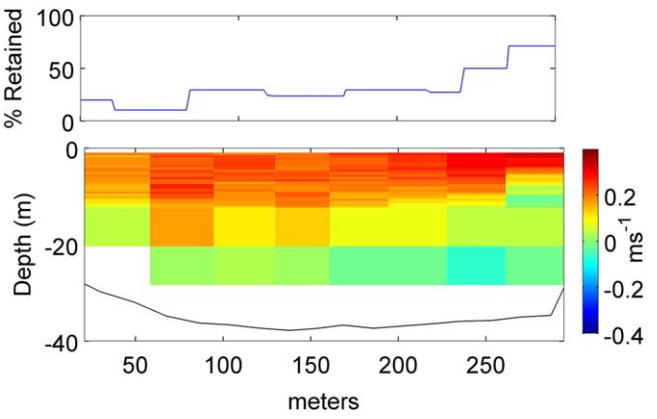

Figure 7. Average velocity in pass cross section. The *x* axis indicates distance along the transect with zero being the westernmost point of the transect line shown in Figure 1. The color shows velocity in m/s. The flux centroid for this velocity distribution is on the right side of the channel at 160 m.

for the setup of the free-surface gradient required to drive the alongshore current. The boundaries that represent the jet and reef were forced with a fixed velocity. Given that the outflow in the jet is determined by the total wave-driven flow over the reef crest, the flow out of the domain through the reef boundary was set to equal the flow into the domain from the jet. The offshore boundary (parallel to the reef crest) was a free-slip, no-flux boundary.

As depicted in Figure 8, the physical dimensions of the grid were chosen to match the geometry of the fore-reef and pass system of Moorea. The "pass" was set to be 300 m wide and 30 m deep and was located in the center of a 7 km wide domain that extended 9 km offshore. The bottom of the domain outside the pass sloped uniformly from 2 m at the reef crest to 200 m, 1.5 km offshore of the reef, and was flat further offshore. This slope matches that of the fore-reef in the field. The size of the domain was chosen to allow full development of the alongshore flow, and to prevent the reef flow from being overly influenced by the offshore wall. The length of the reef crest, where the flux boundary condition was applied, is 1 km on each side of the jet to reflect the channel spacing in Moorea (2–3 km apart). The grid had 5 m resolution in the horizontal and when buoyancy forcing was included, a stretched grid in the vertical having 20 cells that were distributed between 3 m at the surface to 20 m at the bottom. At the reef outlet, there was a single 2 m deep cell and at the pass input there were seven vertical cells. With a time step of 2 s dictated by the Courant condition related to explicitly computed momentum and scalar advection, each simulation ran for a minimum time of 20,000 s (10,000 time steps) until a steady state velocity field was achieved. All results reflect the steady state solution. Table 2 shows the parameters used for the runs performed in this paper.

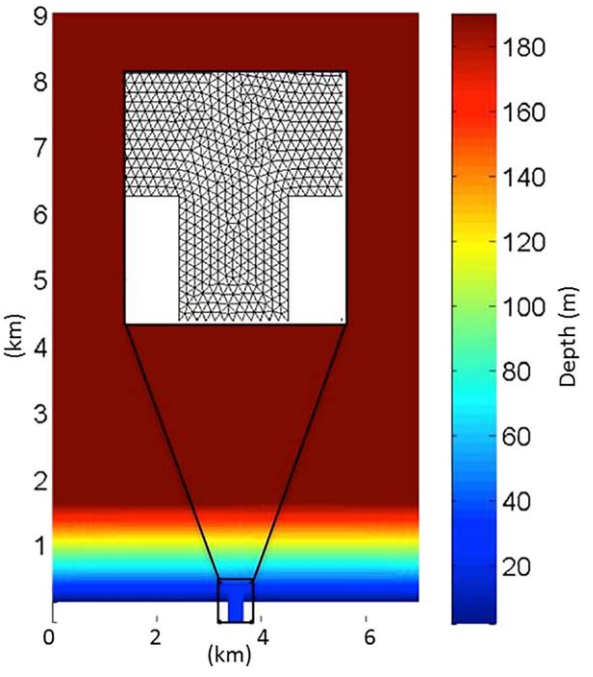

Figure 8. SUNTANS model domain: a 9 km by 7 km rectangle with a 300 m^2 channel centered on the southern wall to form the pass jet. The color indicates the depth in meters. The inset shows a close up of the individual cells.

3.3. Nonbuoyant Runs

In the first set of runs (runs 1–10 in Table 2), the alongshore velocity was varied for a non-buoyant jet. The jet velocity was 0.15 ms^{-1} while the alongshore velocity ranged from 0 to 0.105 ms^{-1} for a ratio of 0 to 0.7 between alongshore velocity and jet velocity.

From Figure 9, it is clear that the jet penetrates farther offshore with weaker alongshore velocity, behavior that is consistent with other studies [e.g., *Jirka*, 2007; *McGuirk and Rodi*, 1978]. However, the shape of the "zone of recirculation," which is defined as the off-shore area of jet fluid that ultimately returns to the reef crest, or remains wall-attached in the absence of a reef, behaves differently in the two cases. In the case shown here, the length of the zone of recirculation is set by the physical length of the reef crest, because the flux at the reef crest forces wall attachment downstream. In some

Table 2. Parameters for Model Runs[a]

Run	V Jet (ms^{-1})	U Alongshore (ms^{-1})	Buoyancy (g')
1	0.15	0	None
2	0.15	0.0075	None
3	0.15	0.015	None
4	0.15	0.0225	None
5	0.15	0.03	None
6	0.15	0.045	None
7	0.15	0.06	None
8	0.15	0.075	None
9	0.15	0.105	None
10	0.15	0.15	None
11	0.1	0.05	2×10^{-3}
12	0.1	0.05	9.8×10^{-4}
13	0.1	0.05	3×10^{-4}
14	0.1	0.05	2×10^{-4}
15	0.1	0.05	9.8×10^{-5}
16	0.1	0.05	2×10^{-5}
17	0.1	0.05	9.8×10^{-6}
18	0.1	0.01	2×10^{-4}
19	0.1	0.02	2×10^{-4}
20	0.1	0.04	2×10^{-4}
21	0.1	0.07	2×10^{-4}
22	0.1	0.1	2×10^{-4}
23[a]	0.1	0.1	2×10^{-4}
24[a]	0.15	0.105	None

[a]Run had no flux at the reef crest.

of the weaker alongshore flow cases, the centerline trajectory passes the end of the reef crest, but turns back to the reef crest since for these nonbuoyant runs we used a depth-averaged model and the flow over the reef crest is set to equal that of the jet. This inability to pass the reef crest without returning, likely over predicts the amount of retention than might be seen in reality. Also, the abrupt end of the flux over the reef crest at a no-flux boundary is not realistic, and creates a sink-like flow field at the end of the reef. In reality, the reef would continue but would feed another source, or there would be another pass with a jet. However, this difference creates small changes in the local flow field and does not affect retention significantly.

The fixed alongshore length scale in the present case means that the shape of the recirculation zone only changes in the cross-shore direction with jet momentum. The continued expansion of the jet offshore with increasing jet momentum is evidence that the far wall of

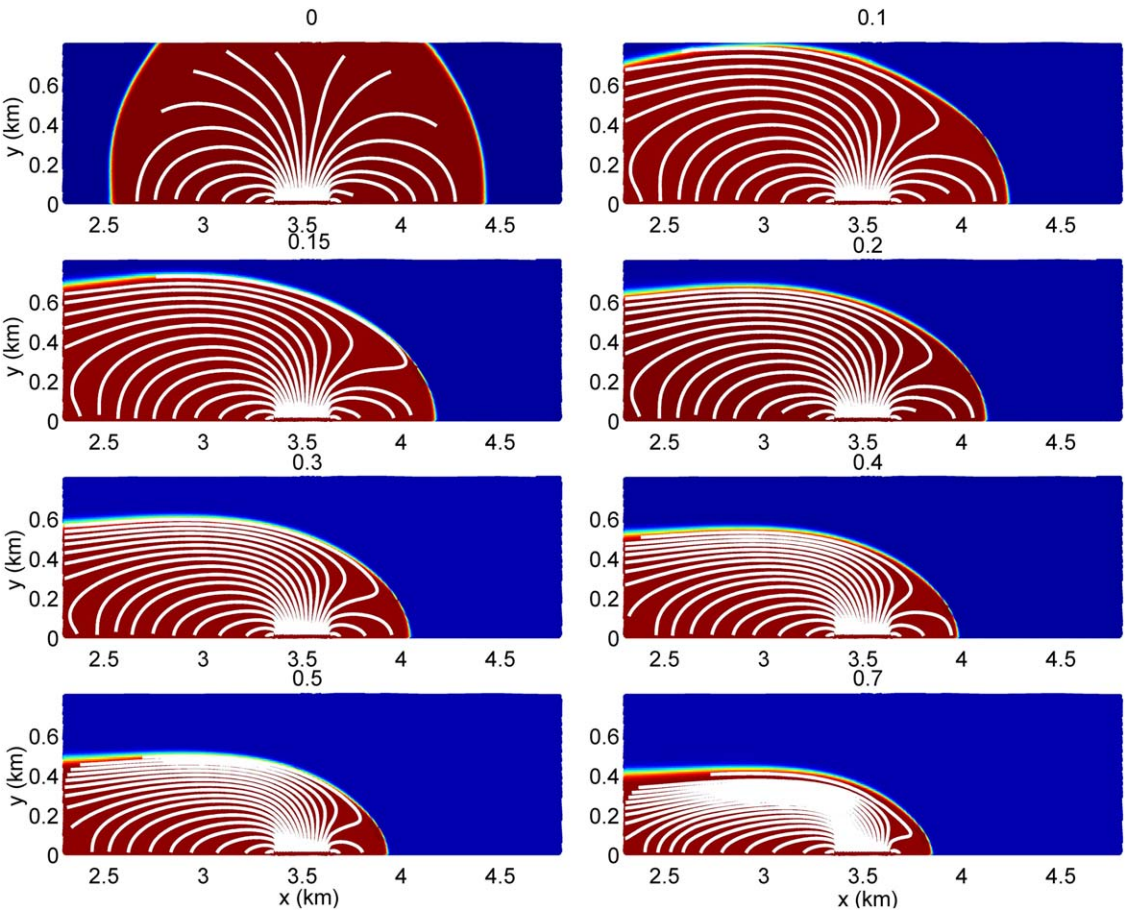

Figure 9. Nonbuoyant jet runs. Each plot show the final distribution of jet water (red) relative to ocean water (blue). The white lines are the paths of particles released at the jet opening in the steady state velocity field at the end of each run. Plots (a–h) correspond to runs 1, 3–9 in Table 2 and are labeled with *R*, the alongshore velocity to jet velocity ratio.

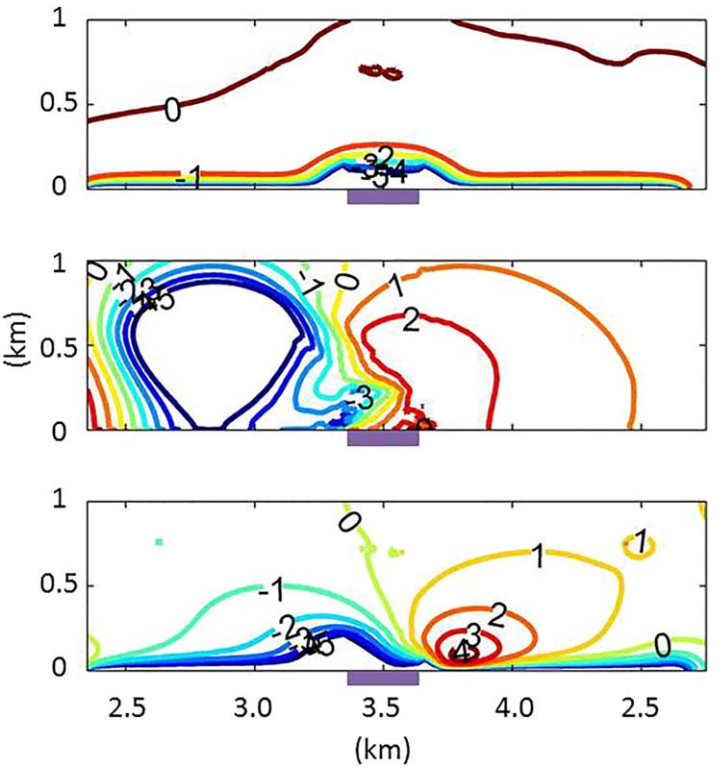

Figure 10. Pressure contours from selected non-buoyant jet runs: (a) a jet and reef-crest with no alongshore flow (run 1; Figure 9a); (b) a jet with strong alongshore flow and no flow over the reef crest (run 24); (c) a strong alongshore flow with a reef crest (run 9; Figure 9h). The purple rectangle below the *x* axis indicates the location of the jet opening.

the domain does not interfere with the evolution of the jet and thus accurately reflects the field case with an open ocean.

The main result from these non-buoyant runs is that we see we are able to predict the shape of the jet by combining simple analysis used in the jet in a cross-flow literature with the additional pressure gradients created by the flow over the reef crest to generate a self-similar jet center line trajectory. As seen in other jet in cross-flow studies, our model results show that the jet turns more sharply with the increased alongshore flow. Jets in alongshore-flow are known to block the alongshore flow creating a high-pressure zone upstream of the jet and a low-pressure zone downstream of the jet. This can be seen in the pressure contours of a run with no reef crest (Figure 10b). In the zero alongshore-flow case, the pressure contours are symmetrical around the jet opening with very strong pressure gradients near the reef crest; these are responsible for driving the flow over the reef crest and out of the domain (Figure 10a). As might be expected, for the jet in cross-flow with flow over the reef crest, a combination of the two pressure gradients: there is a high-pressure zone on the upstream end of the jet and a low pressure zone on the downstream end of the jet, but the effect of the reef is to compress these pressure variations into a region that is closer to shore. The low-pressure zone of the jet combines with the low-pressure zone of the reef crest and appears to be flattened against the edge of the reef crest.

Generally, the momentum balance for the nonbuoyant jets is primarily between advection of momentum and the pressure gradient provided by the free surface (Figure 11). Analysis of the momentum balance for the midlevel *R*-value case ($R = 0.3$) we found in the cross-shore direction pressure and momentum advection balance each other with a negligible contribution from friction. In the alongshore, pressure and advection of momentum make up the main balance in most of the domain, however in the shallowest parts of the domain near the jet opening and reef crest friction is important. The free surface gradient is important in maintaining the flux into the domain via the jet and out of the domain over the reef crest.

These model runs represent the combination of two flow behaviors: The simpler case of a jet in a cross-flow and a jet exiting reef pass can both be described by a pressure-inertia balance. This suggests that a self-similar scaling for the trajectories of a jet with a cross flow and an entraining reef crest might be possible. In Figure 12a, we see the raw centerline trajectories from the jet. In Figure 12b, the same trajectories from the jet are scaled with the momentum scaling given in *Jirka* [2007]

$$L_y = \frac{M^{0.5}}{U_a} \tag{4}$$

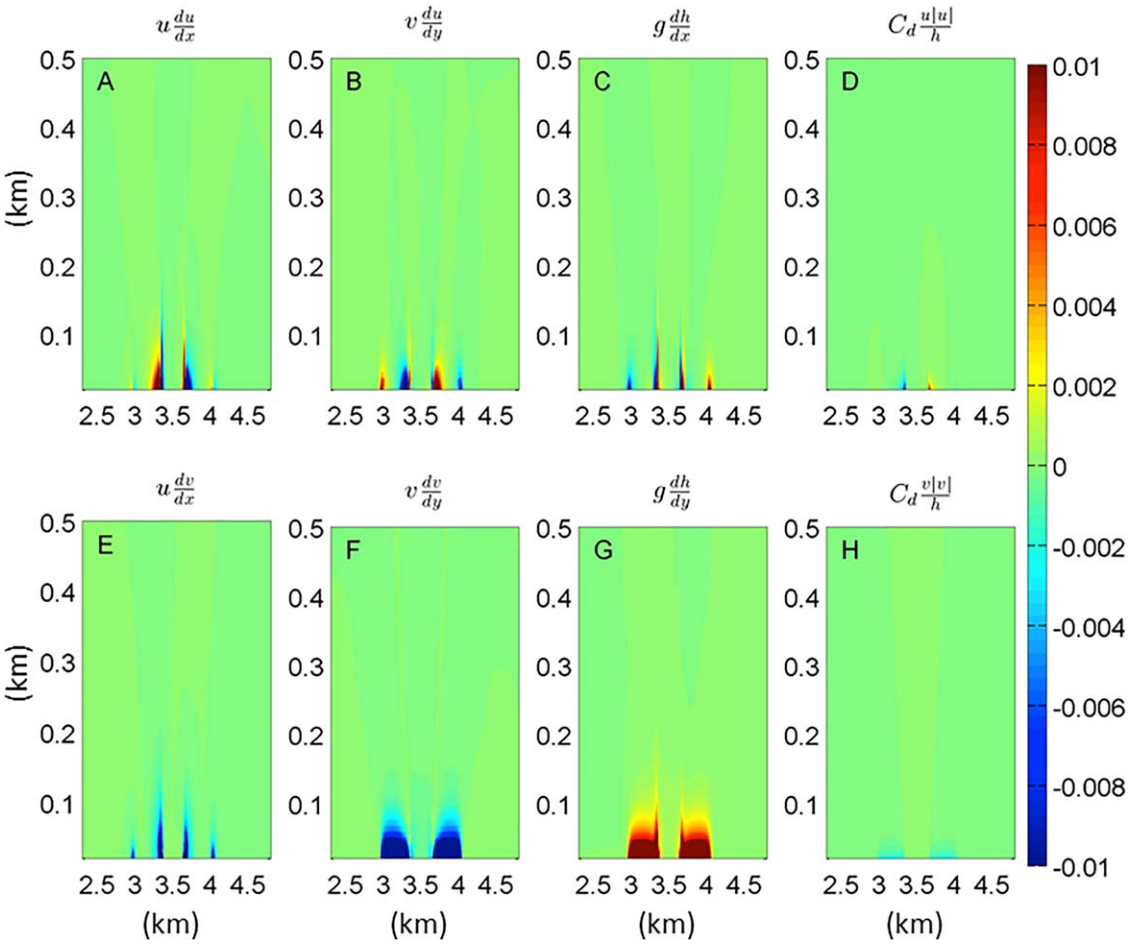

Figure 11. Momentum balance of nonbuoyant jet runs. (a–d; top row) Momentum balance along the *x* direction. (e–h; bottom row) Momentum balance along the *y*-direction. The jet-opening is centered at 3.5 km.

where $M=U_j^2bh$ is the flux of momentum calculated using, the jet velocity, U_j, jet width, b, and jet depth, h. As seen in Figure 12b, this scaling overpredicts the maximum offshore distance of the jet substantially and does not collapse the trajectories onto a single dimensionless curve. Evidently, equation (4) is not appropriate for the reef jet flow.

However, we can alter equation (4) to correct for the additional low pressure from the reef pass by creating an effective ambient velocity U_g corresponding to the alongshore flow that would decrease the pressure an amount equivalent to the pressure decrease required to drive the reef crest flow. U_g was found for our model runs by fitting the free surface deflection in the lee of the jet to a quadratic function of velocity (per the Bernoulli equation), giving $U_g = 0.08$ ms^{-1}, a constant since all of the model runs were done with the same flow over the reef crest, In terms of this extra velocity, we alter equation (4) to read:

$$L_y^* = \frac{M^{0.5}}{(U_a + U_g)} \tag{5}$$

As seen in Figure 12c, using the scaling shown in equation (5), all the computed trajectories collapse onto a single dimensionless trajectory.

Thus, effectively summing the pressures in the lee of the jet, one due to jet blocking and the other related to the low pressure required to drive flow over the reef crest, we can predict the amount of jet bending that will occur. This should not be a surprise since *Jirka* [2007] showed that the Bernoulli equation could be used to predict the blocking effect.

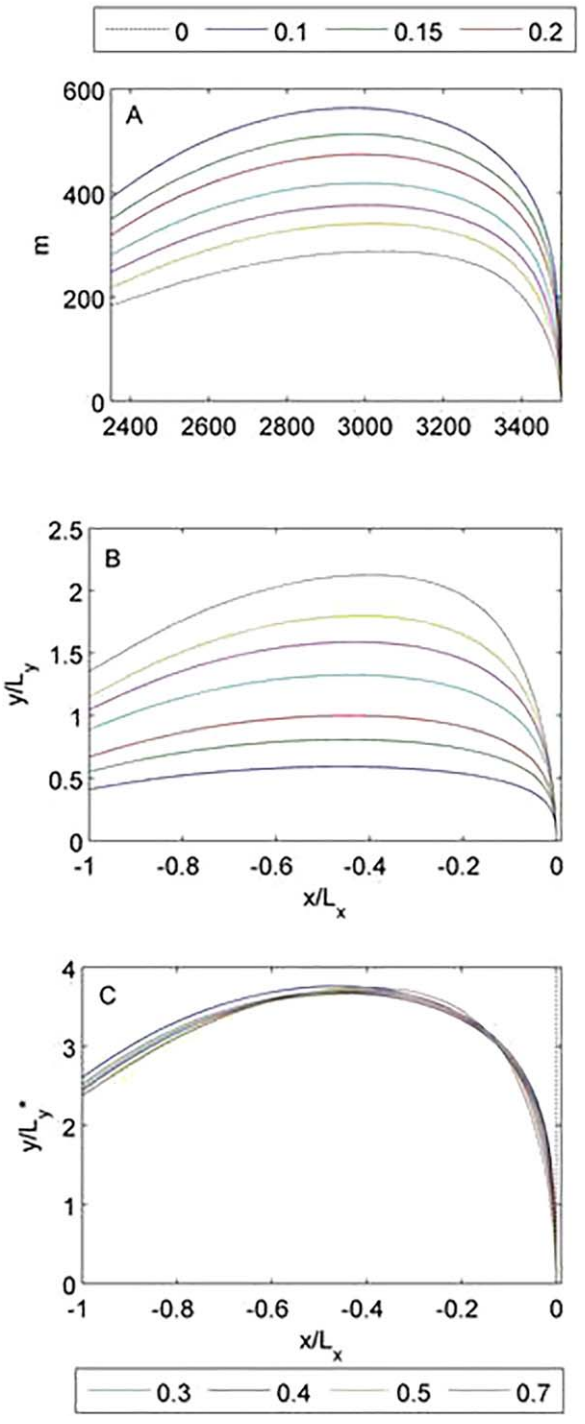

Figure 12. Centerline trajectories of the jets shown in Figure 8: (a) unscaled trajectories; (b) trajectories scaled by the reef length in the *x* direction and in the *y* direction by the jet scale defined by equation (4); and (c) Jet trajectories scaled the modified *Jirka* scaling given by equation (5). In each case, the legend gives values of *R*.

3.4. Runs With Buoyancy

The other parameter that we varied was the density of the jet, thus varying the internal Froude number of the jet, F_{jet}. In our model runs with buoyancy $0.4 < F_{jet} < 5.8$ where F_{jet} is based on the initial jet velocity, initial jet depth (30 m), and the buoyancy difference of the jet compared to the ambient water. Each scenario was run for at least 10^4 s, i.e., ≈3 h. The scalar field and trajectories from these runs, where F_{jet} and U_a/U_j were varied, can be seen in Figure 13. Unlike the runs without buoyancy, steady state was not reached over the entire domain by the end of these runs. However, steady state was reached with respect to the fate of the jet water, i.e., the fraction of jet fluid that exited at the reef crest boundary. Thus, while in many runs the leading edge of the front was still propagating offshore, the dynamics of the near-shore region were no longer changing substantially.

With buoyancy, the jet water goes much farther offshore and the scalar field near the reef crest shows lower concentrations as compared to the 2-D case. This is because the jet separates from the reef as it goes downstream. Ambient fluid is entrained under the plume and onto the reef (Figure 14). In the lowest Froude number cases, the spatial distribution of jet water is much more symmetric with respect to the pass, jet water intrudes far upstream. The trajectories of the particles that leave from the mouth of the jet appear to get caught in the edges of the front offshore, which results in sharp turns in particle path lines (Figure 13). Sharp turns like this were observed in many of the field drifter releases (Figures 5b, 5e, 5i, and 5m) indicating the importance of buoyancy to the fate of surface-trapped particles.

With buoyancy, the effect of alongshore flow is weaker when compared to cases with the same velocity ratio U_a/U_j but with no buoyancy. Even the highest Froude number case (F_{jet}=5.8) does not stay bottom-attached, and so even in this case, the offshore jet evolution is different from the nonbuoyant case. The lower Froude number flows lift off from the bottom closer to the pass allowing more alongshore water to pass underneath the buoyant jet. In these runs lift-off depth varied inversely with the initial Froude number, just as found in *Atkinson* [1993].

Separation of the jet from the bottom minimizes the blocking effect, changing the mechanism for the alongshore flow turning the jet from one involving the pressure gradient (i.e., blocking) to one involving

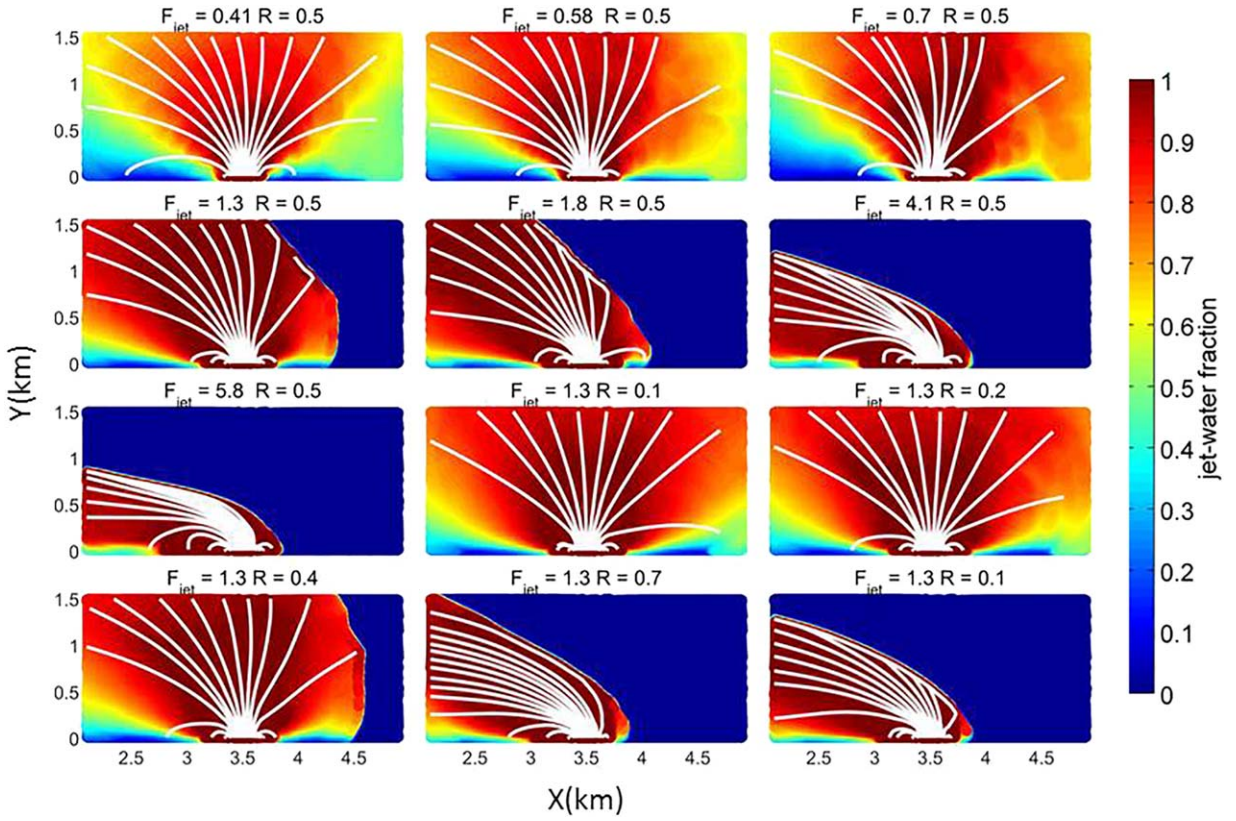

Figure 13. Trajectories and surface scalar fields for buoyant jets. Particle trajectories are for particles released at the jet opening and integrated through the top layer velocity field. Red is jet water and blue is ocean water. Each run is labeled with the internal Froude number of the jet and the alongshore velocity. The exiting jet velocity was the same (0.1 ms^{-1}) for every run.

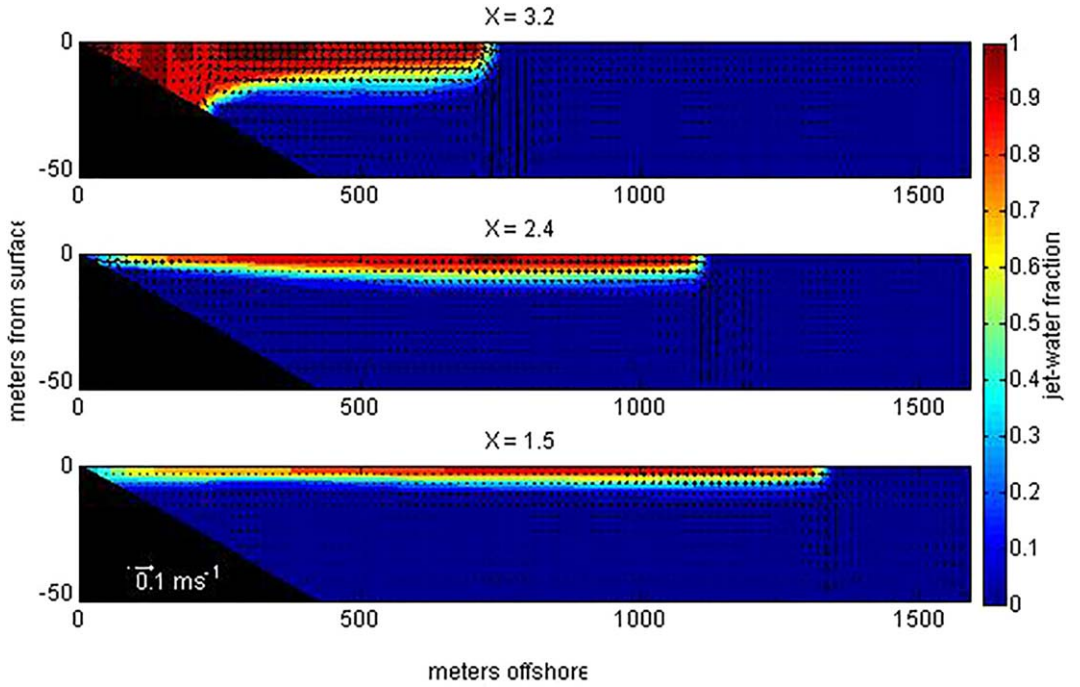

Figure 14. Offshore transects of jet water for F_{jet} = 1.3 and R = 0.01: (a) At X = 3.2 km (just downstream of pass); (b) At X = 2.4 km mid reef; and (c) At the downstream end of the reef at X =1.5 km. The color indicates the concentration of jet fluid and the arrows show the velocity in vertical and cross-shore directions with the scale shown in the lower left of Figure 14c.

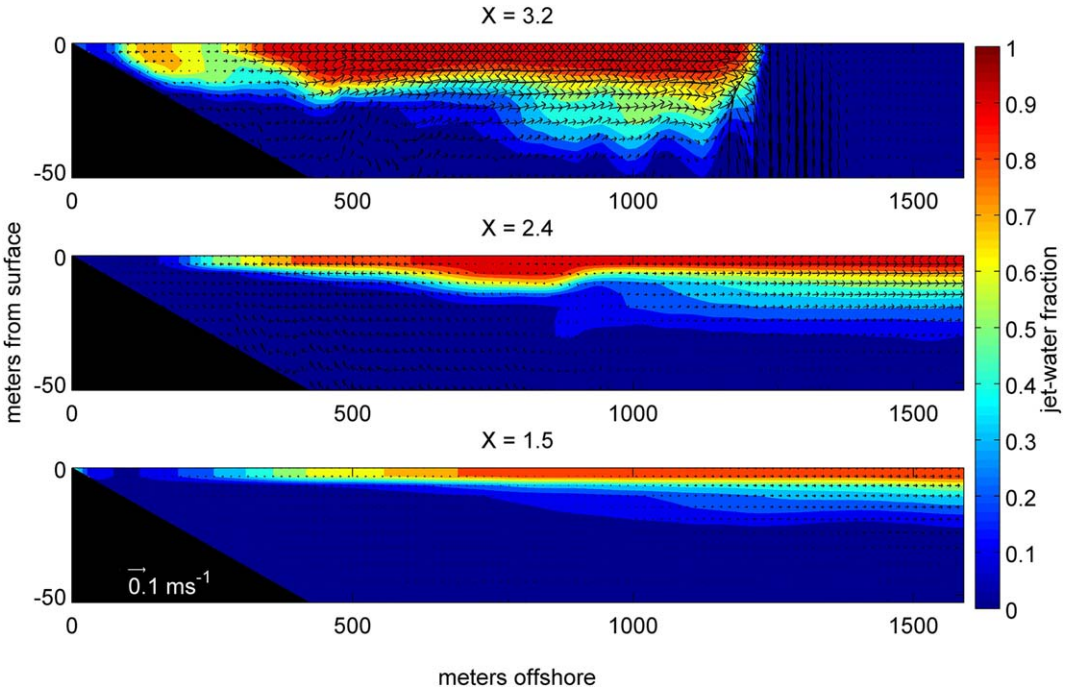

Figure 15. Same as figure 14 but with the no flow over the reef crest.

the entrainment of alongshore momentum. In the scalar field along the center trajectory, we find evidence for the different turning mechanisms: in the two-dimensional case, there is absolutely no reduction of scalar concentration indicating that there is no entrainment of ambient fluid so the bending of the jet centerline is solely from pressure field. In the cases where buoyancy is included, the scalar concentration along the jet-center streamline decays with a dependence on F_{jet}. For the majority of runs, the concentration begins to decay between 10 and 20 times the jet to plume length scale. For the high F_{jet} (5.8 and 4.1) cases, the decay begins between 1 and 2 jet to plume length scales.

Unlike the two-dimensional case, the centerline paths do not collapse on to a single dimensionless trajectory. This is likely due to the fact that force balance changes along the trajectory [see *Fischer et al*., 1979]. The relative importance of momentum and buoyancy vary along the centerline of the jet. Moreover, the runs with smaller values of R are outside the range of velocity ratios analyzed by *Jirka* [2007]. *Jirka* found that the length, L, of the zone of flow establishment, where channel geometry strongly influences flow characteristics, for buoyant surface jets entering perpendicularly into a crossflow takes the form:

$$L = \sqrt{bh}\left(1 - \frac{3.22}{R}\right)e^{-5/F_{jet}^2} \tag{6}$$

For the values of R we modeled, i.e., when $R < 3.22$ equation (6) gives the nonphysical result that $L < 0$. This indicates that the range of parameters relevant to the reef span a region where different dynamics are at play in establishing the initial flow conditions and that Jirka's parameterization will not be applicable. Different scaling is required to parameterize the structure of the relatively weak jets we consider here. Moreover, given that flows at the exit from Avaroa Pass can be both jet-like or plume-like or somewhere in between (Figure 16), we should not expect that a single scaling would suffice to describe such flows.

However, the behavior seen in the two-dimensional case, i.e., the reef sink enhances turning of the jet downstream of the source still occurs. The difference is that the buoyancy minimizes the blocking effect, creates a pressure gradient that acts to spread the jet water offshore more quickly, and permits entrainment of ocean water from underneath the plume. These mean that the reef sink, although still producing a substantial free surface gradient, produces less downstream reattachment in the buoyant case and the fluid in the plume that is entrained over the reef is a mixture of jet fluid and ocean water. Thus, the net effect of buoyancy in the jet is to produce less recirculation of jet fluid.

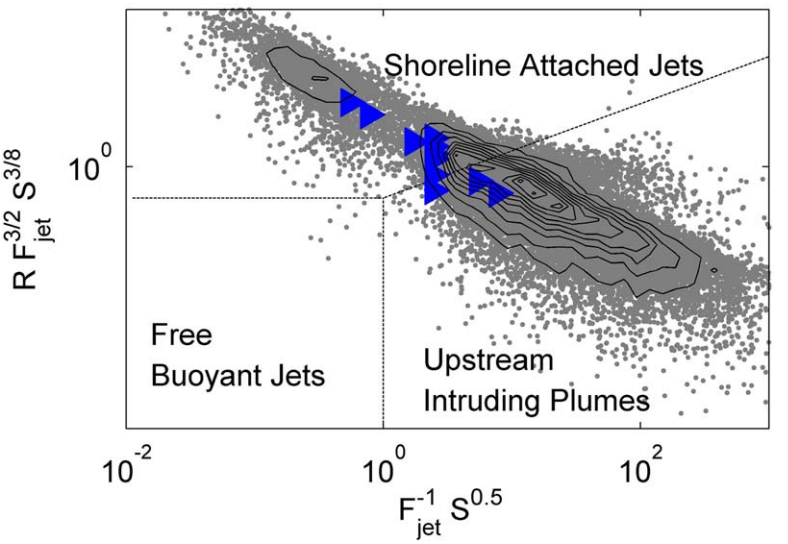

Figure 16. Classification of jets and plumes in terms of length-scale ratios given by *Jirka* [2007] recast in terms of the dimensionless variables given in equations (1)–(3). The grey dots show the values for the field data with the contours indicating density of points. The blue triangles show the values for the simulations including buoyancy.

This behavior can be seen in Figures 14 and 15 cross-shore sections through the jet at different points along the downstream reef, both with a reef cross flow (Figure 14) and without a reef cross flow (Figure 15) but otherwise the same conditions. Without the flow at the reef crest, the leading edge of the jet makes it offshore faster and the body of the jet does not stay attached to the reef crest for the entire length of the reef. The most obvious impact of the reef flow is seen immediately downstream of the pass where a greater portion of jet water is wall and bottom attached than in the absence of flow across the reef crest.

The flow at the reef crest and the associated pressure gradients also change the development of the leading edge of the plume. In the absence of reef flow, there is a larger amount of mixed water under the leading edge of the jet along with internal waves traveling along the interface. Thus, the flow over the reef crest affects the jet behavior offshore. By the midpoint of the downstream reef, the jet in the no reef flow case has completely separated from the wall (Figure 15b), while the case with reef flow (Figure 14b) is still entraining jet fluid at the reef crest, albeit as a mixture of ocean and jet water. At the end of the reef both plumes are similar in depth and length, although in the presence of the flow over the reef crest, the mixed-density water stays adjacent to the reef crest while in the absence of the flow over the reef crest the inshore edge of the plume is 250 m offshore of the reef crest. Thus, the effect of the reef crest flow is to compress the development of the jet/plume against the reef and create greater retention of jet water in the reef system, as opposed to the case of no reef crest flow for which buoyancy has the tendency to spread off-shore, thus minimizing the retention of the jet water in the reef system.

4. Discussion

4.1. Regime Behavior

We can examine our data in terms of the regimes defined by *Jirka* [2007], finding that our observations and our simulations fall on the boundary separating upstream intruding plumes from shoreline attached jets (Figure 16). Most of the simulations fall in the shore-line attached jet region, although the lowest Froude number and lowest alongshore velocity cases would be classified as upstream intruding plumes according to Jirka. The lowest alongshore velocity case modeled with a Froude number of 1.3 (shown in Figure 13h) is on the border between the two regimes in Figure 16.

Overall, the scalar fields and trajectories shown in the buoyant runs in Figure 13 generally show significant upstream intrusion and behave more like upstream intruding plumes than shoreline attached jets as defined by *Jirka* [2007]. Thus, the effect of the reef crest is to shift the region of the upstream intruding plumes to higher Froude numbers than was found by Jirka. This is because the pressure field driving the

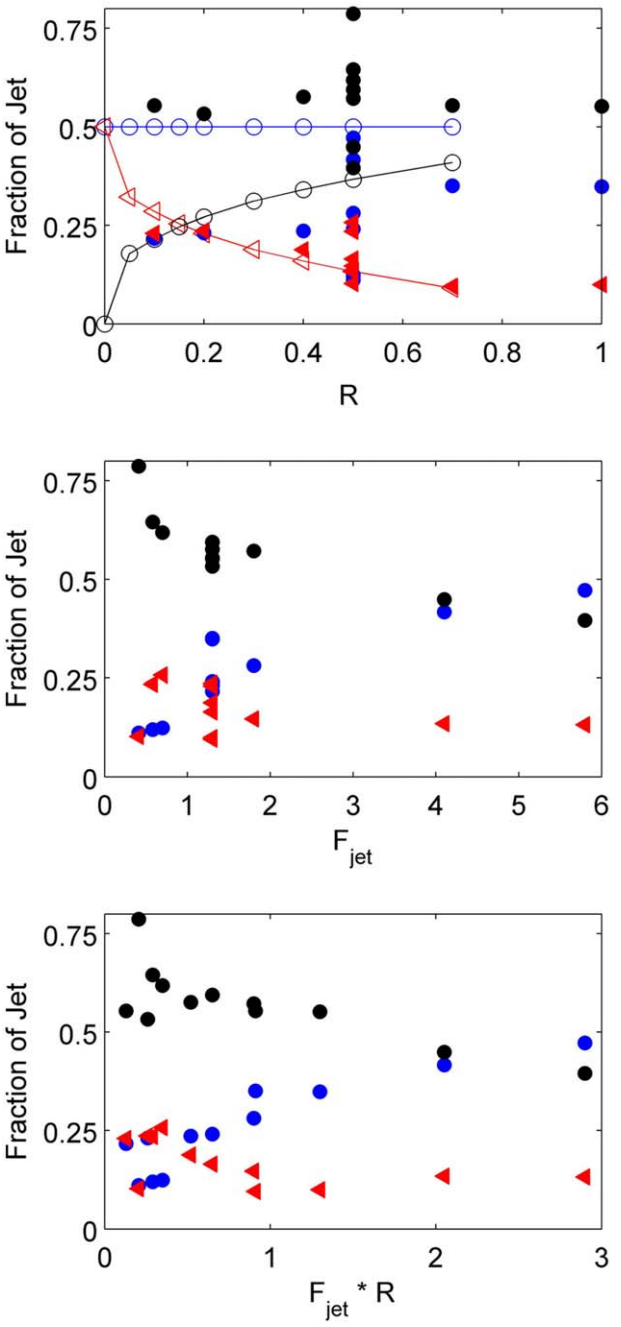

Figure 17. Jet retention as a function of: (a) velocity ratio, R; (b) Jet internal Froude number, F_{jet}; and (c) the combined parameter $F_{jet}R$. The black dots indicate the fraction of the jet water that is not recirculated over the reef crest whereas the blue dots indicate the fraction of water that is recirculated into the downstream reef. Red triangles indicate the fraction of jet fluid that enters the upstream reef. In Figure 17a, the unfilled points connected by a line are the data for the model runs with no buoyancy or an infinite Froude number.

reef flow enhances the symmetrical spreading of the jet as it exits; by compressing the pressure field associated with jet-blocking it lessens the effect of the alongshore flow, thus allowing the spreading associated with the buoyancy to dominate. In effect, flows with low buoyancy and a reef sink resemble cases of buoyant jets with higher buoyancy near a wall.

4.2. Model Jet Retention Compared to Observations

Ultimately, what we are interested in is how these changes in pressure, velocity, and jet shape change the amount of jet water recirculated back over the reef crest, i.e., how the dynamics of the jet/sink combination affects residence time for the reef system. Figure 17a shows how the fate of the water varies as U_j/U_a changes for both buoyant and nonbuoyant simulations. By design, in the nonbuoyant cases, 50% of the water always goes over the downstream reef crest. The amount of water that escapes the domain increases with increasing alongshore flow velocity. This is a result of the alongshore flow compressing the pressure gradient on the upstream side of the jet and minimizing the amount of water that returns via the upstream reef crest. We see that at a minimum, with no buoyancy, the flow over the upstream reef crest pulls 10% of the jet water with it. This indicates that a maximum of 40% of the jet water escapes the domain. This is a much higher fraction of retention than we observed using drifters. The addition of buoyancy decreases the fraction of outflow that is reentrained, thus more accurately reflecting our field observations. In the simulations with buoyancy, between 50 and 80 percent of the jet water escapes the reef system. Nonetheless, as in the nonbuoyant cases, for buoyant cases we also find that increasing the alongshore flow decreases retention by the upstream reef. However, in the buoyant cases, this also increases the retention in the downstream reef crest. This means that for a given amount of buoyancy the total retention does not change as much with changes in alongshore flow as in the nonbuoyant bottom attached case.

In Figure 17b, we see how the retention changes with Froude number. The high Froude number cases are similar to the comparable nonbuoyant case ($U_j/U_a = 0.5$) when half of the jet flow went over the

downstream reef and only 13% went over the upstream reef. The highest buoyancy case ($F_{jet} = 0.41$) distributes the retention differently: almost equal amounts of water enter the up and downstream reefs in the highest buoyancy case while, in the next most buoyant case ($F_{jet} = 0.58$) more jet water returns via the upstream reef crest. For weaker buoyancy, the results asymptote to the nonbuoyant case for which 50% of the water is retained by the downstream reef crest. The primary explanation for the lower retention with buoyancy is that in the presence of buoyancy, the jet separates off of the bottom and "new" ocean water mixes with the jet before it returns over the reef crest. Also the buoyancy helps push the jet offshore and minimizes the effects of the alongshore velocity. This shows that although the buoyancy increases retention on the upstream side of the jet it is insufficient to overcome the decreased retention on the downstream side of the jet. In summary, the overall trend is that more buoyancy creates less retention.

The last parameter that we consider as influencing retention is the product of F_{jet} and R,

$$F_{jet}R = \frac{U_a}{\sqrt{g'h}} \tag{7}$$

This parameter effectively defines an internal Froude number based on the ambient flow and the internal wave speed associated with conditions existing at the source in the pass. In Figure 17c, we see that when $F_{jet}R > 1$ downstream retention increases with $F_{jet}R$ while the upstream retention remains constant at about 10%. When $F_{jet}R < 1$, the relationship is more complicated. It appears that there are competing effects between the tendencies for jet water to intrude upstream as opposed to spreading offshore. The effect of these competing effects is to create a local maximum in retention at $F_{jet}R \cong 0.5$.

Our field observations are best replicated by model runs with low Froude numbers and low velocity ratios. The shape parameter of course did not change at the field site and thus we maintained a constant S =10 in our model as well. The distribution of those parameters over the 9 months we took measurements in terms of the scaling parameters are shown in Figure 16, where it can be seen Froude numbers near 1 are common. The velocity ratio U_a/U_j was less than 2 for 90% of the time. This places our field site on the low range of all three independent parameters shown in Figures 17a–17c, and thus suggesting that, as observed, 30–50% of the jet will be retained by the system and that higher rates of retentions will be very rare.

4.3. Other Variables That Affect Retention

Two reef geometry parameters that might affect retention and recirculation zone dynamics but were not specifically examined here are the aspect ratio of the jet and the bottom drag coefficient. A higher width to depth ratio of the jet would likely decrease the penetration distance because bottom drag would be stronger relative to the momentum of the jet when the jet is bottom attached. The drag coefficient used in the modeling was $C_D = 0.005$, a value that is lower than has been observed for the Moorea fore-reef [*Monismith et al.*, 2013] as well on other coral reefs [e.g., *Lowe et al.*, 2009a,2009b]. In the two-dimensional cases, a larger drag coefficient and hence stronger bottom friction would require larger pressure gradients to drive the flow over the reef crest. Increased friction will also lower the effect of jet blocking in the near field because the alongshore velocity would be lower in the shallow area near the reef crest. However, the results of one buoyant jet run with $C_D = 0.05$ were not substantially different from the case where $C_D = 0.005$. In the buoyant cases the jet separates off the bottom, even with very small buoyancy differences, causing bottom friction to have a minimal impact on jet shape and recirculation.

The addition of unsteadiness in either the ambient flow or in the jet conditions could also affect retention etc. In particular, the time scales to develop the offshore recirculating flow can be longer than the time scales over which the alongshore flow is steady, particularly around times of current reversals. In this case, the Moorea jet may be unusual in that it has little tidal variability [*Hench et al.*, 2008], as opposed to other systems, e.g., Kaneohe Bay [*Lowe et al.*, 2009a] for which tides can be important. While it is beyond the scope of the present work, it would be interesting to see how retention/recirculation etc., change with unsteady jet conditions and time-varying alongshore currents.

Our model has been simplified by not explicitly including surface waves, instead representing their effect only through the net flow they drive. We believe that had we explicitly included waves, the results would not have been significantly different. First, advection of offshore fluid toward the reef crest would be similar in both cases since, by construction, the depth-averaged mean Lagrangian velocity on the fore-reef would be the same in both cases. Second, wave current interactions in the jet, as computed by the vortex force

[*Uchiyama et al*., 2009] from the spatial velocity field generated by the drifters can be shown to be generally an order of magnitude smaller than the other terms in the jet momentum balance (shown in Figure 11). In either case, the mean momentum balance requires that the free surface slope balance both bottom friction and spatial acceleration. The former is generally unimportant on the fore-reef. The latter, which is only important if the fore-reef is steep, is the same in both cases since it is the acceleration of the mean Lagrangian flow, something that depends inversely on depth and is the same in both cases. Thus, the low pressure zones created near the reef pass and reef crest will be similar to those shown in the model results. Third, while in general waves can significantly modify the bottom stresses acting on the mean flow, our observations [*Monismith et al*., 2013] showed little explicit effects of waves on along-reef flow structure suggesting that roughness effects associated with the reef spur and groove structure may be more important than waves in setting fore-reef bottom stresses.

While the mean advection toward the reef crest is the same with and without explicit waves, the biggest discrepancy between the two cases is likely due to the fact that the idealized model has relatively constant velocities with depth, while in deeper water, the mean onshore Lagrangian flow is likely to be more vertically sheared since the Stokes drift will be stronger near the surface than at depth. This would tend to preferential draw surface waters, i.e., offshore jet fluid toward the reef crest, thus weakening the extent to which buoyancy reduces retention. Nonetheless, we believe this is a secondary effect compared to the fact that by including buoyancy we were able model significant patterns in the drifter releases, e.g., sharp turns in drifter trajectories along the buoyancy fronts at the edges of the jet. Thus, it is clear that the net impact of buoyancy must be to reduce retention, although the strength of this effect may be altered by the strength of the wave forcing.

The other issue for predicting the amount of water recirculated from jet to reef crest is the rate of entrainment of ocean water into the jet as it is recirculated off-shore. This is an issue that we are unable to address in detail in this paper, however, it clearly has an impact on predicted recirculation rates. In previous studies of tidal buoyant surface jets the most entrainment occurred behind the leading front. [*Luketina and Imberger*, 1989, 1987] In a more slowly varying unsteady jet such as this, there is not likely to be a strong leading front (called a roller in *Luketina and Imberger* [1989, 1987]) but a series of small subfronts as the jet momentum changes with the transient wave-forcing. There is also strong mixing and entrainment in the lift-off zone of the jet [*MacDonald and Geyer*, 2004; *McCabe et al*., 2010]. And there can also be entrainment associated with regions of shear instability [*Orton and Jay*, 2005]. For these processes, parameters relating buoyancy, friction, and momentum are also important and we hope to be able to examine the role of variable entrainment on net recirculation in the future.

4.4. Residence Times

Using the results above for retention, we can estimate the changes in overall residence time with jet and ambient flow parameters. Classical control volume analysis of a continuously mixed system shows that the time evolution of the concentration is described by the relation:

$$\frac{dC}{dt} = \frac{Q}{V}C_{in} - \frac{Q}{V}C \tag{8}$$

where C is the concentration of the material of interest inside the control volume, V is the volume of the body of water, Q is the flow through the system, and C_{in} is the concentration entering of material entering the volume. If we assume a return flow bQ, from the jet into the system we can estimate C_{in} as:

$$C_{in}Q = C_a(Q - bQ) + CbQ \tag{9}$$

where C_a is the ambient inflow from the ocean, combining with the return flow to get the total flux in. If we assume that the ambient concentration is 0, then

$$C = C_o exp\left(\frac{-Q(1-b)}{V}t\right) = C_o exp\left(\frac{-t}{\tau}\right). \tag{10}$$

Equation (10) shows that the larger the return flow, the more slowly the concentration will decay, i.e., the longer the residence time, τ. The assumption that the system is instantly and continuously mixed might certainly be questioned, but equation (10) shows that b can change the estimate of the residence time

substantially. For the field case with the least recirculation ($b = 23\%$) only 10% of the original material is still in the lagoon system after three flushing times, however in the highest recirculating case, where $b = 50\%$, 10% of the original material is left after five flushing times.

In previous work [*Herdman*, 2012; *Hench et al*., 2008], flushing times for the Moorea reef system were estimated given seasonal variations in wave-driven flow and have been found to range from 0.6 to 9 h. Taking the extremes of these estimated flushing times, this means that the range of residence times for 10% of the water will range between three and five times that, i.e., 1.8 and 45 h. Thus, as would be expected, the fraction of return flow can have a significant impact on the residence time.

5. Conclusions

The observations and modeling we present here show two important features of wave-driven circulation through a barrier reef-lagoon system: (1) The flow over the reef crest that supplies the flow through the reef system has a dramatic effect on the trajectory of the jet/plume that emerges from the pass, such that reentrainment of jet fluid can be as a high as 50%; and (2) Jet buoyancy also has a dramatic effect on jet/plume behavior, tending to act to reduce recirculation of fluid exiting the reef pass through the reef system.

The behavior of this jet/plume can have important consequences for the biogeochemical and ecological functioning of the reef system. First, any biogeochemical or ecological process that depends on residence time will vary with wave conditions and with whatever acts to change the density of fluid exiting the pass, in our case, heating. Indeed, because of differences in depth between the offshore ocean and the reef system, the water flowing in from the ocean can heat up substantially on the shallow back-reef due to solar radiation [*Koweek et al*., 2015], so the longer the residence time, the greater the temperature difference that can develop between the reef and the offshore ocean [*Herdman et al*., 2015]. Thus, the jet/plume behavior studied here clearly provide a mechanism for negative feedback: given that the net ocean-lagoon exchange rate (inverse of retention) increases when reef waters become warm (buoyant), residence time would tend to decrease with heating, moderating the increase of shallow reef temperatures relative to ambient ocean temperatures.

Second, depending on jet/plume buoyancy, the distance offshore the plume travels in the near field can influence the degree to which different, nearby reef systems are "connected" to each other. That is, jet/plume water that makes it sufficiently far offshore to enter the prevailing longshore current system will transport materials, e.g., planktonic larvae, away from the source reef. At our site on Moorea, this generally would mean transport to the next reef-lagoon system 4 km to the west, although, given the complex flows known to exist in the Society Islands, it also could result in transport to other nearby islands.

Acknowledgments

We thank Kristen Davis, Jamie Dunckley, Robert Driscoll, Sarah Giddings, Nick Nidzieko, Johanna Rosman, and Michael Squibb for help with the field measurements. Bing Wang provided vital help with the modeling. Olivia Cheriton and an anonymous reviewer provided helpful comments that greatly improved the manuscript. Support for this work came from the National Science Foundation through the Moorea Coral Reef LTER (OCE-0417412; OCE-1026851) and Physical Oceanography (OCE-0622967; OCE-1435133; OCE-1536502) programs, and from the Singapore Stanford Partnership. L.H. gratefully acknowledges the fellowship support provided by the ARCS foundation. The data used in this publication are available by contacting Liv *Herdman* (lherdman@usgs.gov) or Jim Hench (jim.hench@duke.edu).

References

Atkinson, J. F. (1993), Detachment of buoyant surface jets discharged on a slope. *J. Hydraul. Eng.*, *119*, 878–894.

Baddour, R., and V. Chu (1986), Surface buoyant jets and plumes, in *Encyclopedia of Fluid Mechanics*, edited by N. Cheremisinoff, Gulf, Houston, Tex.

Black, K. P., S. L. Gay, and J. C. Andrews (1990), Resident times of neutrally-buoyant matter such as larvae, sewage or nutrients on coral reefs. *Coral Reefs*, *9*, 105–114.

Callaghan, D. P., P. Nielsen, N. Cartwright, M. R. Gourlay, and T. E. Baldock (2006), Atoll lagoon flushing forces by waves. *Coastal Eng.*, *53*, 691–704.

Casulli, V., and R. A. Walters (2000), An unstructured grid, three-dimensional model based on the shallow water equations, *Int. J. Numer. Methods Fluids*, *32*, 331–348.

Casulli, V., and P. Zanolli (2005), High resolution methods for multidimensional advection–diffusion problems in free-surface hydrodynamics, *Ocean Modell.*, *10*, 137–151.

Chant, R. J. (2011), Interactions between estuaries and coasts: River plumes–their formation, transport, and dispersal, in *Treatise on Estuarine and Coastal Science*, Elsevier, doi:10.1016/B978-0-12-374711-2.00209-6.

Charpy, L. (2001), Phosphorus supply for atoll biological productivity, *Coral Reefs*, *20*(4), 357–360.

Chu, V. H., and M. S. T. Abdelwahed (1990), Shore attachment of buoyant effluent in strong crossflow, *J. Hydraul. Eng.*, *116*(2), 157–175.

Davis, K. A., S. J. Lentz, J. Pineda, J. T. Farrar, V. R. Starczak, and J. H. Churchill (2011), Observations of the thermal environment on Red Sea platform reefs: A heat budget analysis, *Coral Reefs*, *30*, 25–36, doi:10.1007/s00338-011-0740-8.

Falter, J. L., R. J. Lowe, Z. Zhang, and M. McCulloch (2013), Physical and biological controls on the carbonate chemistry of coral reef waters: Effects of metabolism, wave forcing, sea level, and geomorphology, *PloS One*, *8*(1), e53303.

Fischer, H. B., E. J. List, R. C. Y. Koh, J. Imberger, and N. Brooks (1979). *Mixing in Inland and Coastal Waters*, Academic, London.

Fringer, O. B., M. Gerritsen, and R. L. Street (2006), Parallel coastal ocean simulator, *Ocean Modell*, *14*, 139–173, doi:10.1016/j.ocemod.2006.03.006.

Galperin, B., L. H. Kantha, S. Hassid, and A. Rosati (1988), A quasi-equilibrium turbulent energy model for geophysical flows, *J. Atmos. Sci.*, *45*, 55–62.

Golbuu, Y., S. Victor, E. Wolanski, and R. H. Richmond (2003), Trapping of fine sediments in a semi enclosed lagoon, Palau, Micronesia, *Estuarine Coastal Shelf Sci.*, *57*, 941–949.
Gourlay, M., and G. Colleter (2005), Wave-generated flow on coral reefs: An analysis for two-dimensional horizontal reef-tops with steep faces, *Coastal Eng.*, *52*, 353–387, doi:10.1016/j.coastaleng.2004.11.007.
Hearn, C. J. (1999). Wave-breaking hydrodynamics within coral reef systems and the effect of changing relative sea level, *J. Geophys. Res.*, *104*, 30,007–30,019.
Hench, J. L., and R. A. Luettich Jr. (2003), Transient tidal circulation and momentum balances at a shallow inlet, *J. Phys. Oceanogr.*, *33*(4), 913–932.
Hench, J. L., J. J. Leichter, and S. G. Monismith (2008), Episodic circulation and exchange in a wave-driven coral reef and lagoon system, *Limnol. Oceanogr.*, *53*, 2681–2694.
Herdman, L. M. M. (2012), Circulation, residence time, and retention in a tropical coral reef, PhD dissertation, 308 pp., Stanford Univ., Stanford, Calif.
Herdman, L. M. M., J. L. Hench, and S. G Monismith (2015), Heat balances and thermally-driven lagoon-ocean exchanges in a tropical coral reef system (Moorea, French Polynesia), *J. Geophys. Res. Oceans*, *120*, 1233–1252, doi:10.1002/2014JC010145.
Horner-Devine, A. R. (2009), The bulge circulation in the Columbia River plume, *Cont. Shelf Res.*, *29*, 234–251, doi:10.1016/j.csr.2007.12.012.
Jirka, G. H. (2004). Integral model for turbulent buoyant jets in unbounded stratified flows: Part I: Single round Jet, *Environ. Fluid Mech.*, *4*(1), 1–56.
Jirka, G. H. (2007), Buoyant surface discharges into water bodies: Part II: Jet integral model, *J. Hydraul. Eng.*,*133*(9), 1021–1036.
Johnson, D., R. Stocker, R. Head, J. Imberger, and C. Pattiaratchi (2003), A compact, low-cost GPS drifter for use in the oceanic nearshore zone, lakes, and estuaries, *J. Atmos. Oceanic Technol.*, *20*(12), 1880–1884.
Johnson, D., and C. Pattiaratchi (2004), Application, modelling and validation of surfzone drifters, *Coastal Eng.*, *51*, 455–471, doi:10.1016/j.coastaleng.2004.05.005.
Jones, G. R., J. D. Nash, R. L. Doneker, and G. H. Jirka (2007), Buoyant surface discharges into water bodies. I: Flow classification and prediction methodology, *J. Hydraul. Eng.*, *133*, 1010–1020.
Koweek, D. A., R. B. Dunbar, S. G. Monismith, D. Mucciarone, C. B. Woodson, and L. Samuel (2015), High-resolution physical and biogeochemical variability from a shallow back reef on Ofu, American Samoa: An end-member perspective, *Coral Reefs*, *34*(1), 339–351 doi:10.1007/s00338-015-1308-9.
Lowe, R. J, J. L. Falter, S. G. Monismith, and M. J. Atkinson (2009a), Wave-driven circulation of a coastal reef-lagoon system, *J. Phys. Oceanogr.*, *39*(4), 873–893.
Lowe, R. J, J. L. Falter, S. G. Monismith, and M. J. Atkinson (2009b), A numerical study of circulation in a coastal reef-lagoon system, *J. Geophys. Res.*, *14*, C06022, doi:10.1029/2008JC005081.
Luketina, D. A., and J. Imberger (1987), Characteristics of a surface buoyant jet, *J. Geophys. Res.*, *92*, 5435–5447, doi:10.1029/JC092iC05p05435.
Luketina, D. A., and J. Imberger (1989). Turbulence and entrainment in a buoyant surface plume, *J. Geophys. Res.*, *94*, 12,619–12,636.
MacDonald, D. G., and W. R. Geyer (2004), Turbulent energy production and entrainment at a highly stratified estuarine front, *J. Geophys. Res.*, *109*, C05004, doi:10.1029/2003JC002094.
McCabe, R. M., P. Estrade, J. H. Middleton, W. K. Melville, M. Roughan, and L. Lenain (2010), Temperature variability in a shallow, tidally isolated coral reef lagoon, *J. Geophys. Res.*, *115*, C12011, doi:10.1029/2009JC006023.
McGuirk, J. J., and W. Rodi (1978), A depth-averaged mathematical model for the near field of side discharges into open-channel flow, *J. Fluid Mech.*, *86*, 761–781.
Mellor, G. L., and T. Yamada (1982), Development of a turbulence closure model for geophysical fluid problem, *Rev. Geophys. Space Phys.*, *20*, 851–875.
Monismith, S. G. (2014), Flow through a rough, shallow reef, *Coral Reefs*, *33*(1), 99–104.
Monismith, S. G., L. M. M. Herdman, S. H. Ahmerkamp, and J. L. Hench (2013), Wave transformation and wave-driven flow across a steep coral reef, *J. Phys. Oceanogr.*, *43*, 1356–1379.
Niiler, P. P., and J. D. Paduan (1995), Wind-driven motions in the northeast Pacific as measured by Lagrangian drifters, *J. Phys. Oceanogr.*, *25*(11), 2819–2830.
Nash, J. D., and G. H. Jirka (1996), Buoyant surface discharges into unsteady ambient flows, *Dyn. Atmos. Oceans*, *24*, 75–84, doi:10.1016/0377-0265(95)00457-2.
Orton, P. M., and D. A. Jay (2005), Observations at the tidal plume front of a high-volume river outflow, *Geophys. Res. Lett.*, *32*, L11605, doi:10.1029/2005GL022372.
Sanford, L. P., W. C. Boicourt, and S. R. Rives (1992). Model for estimating tidal flushing of small embayments, *J. Waterway Port Coastal Ocean Eng.*, *118*, 635–654, doi:10.1061/(ASCE)0733-950X(1992)118:6(635).
Stommel, H., and H. G. Farmer (1952), On the nature of estuarine circulation, WHOI technical report, 52–88, Woods Hole Oceanogr. Inst., Woods Hole, Mass.
Uchiyama, Y., J. C. McWilliams, and J. M. Restrepo (2009), Wave-current interaction in nearshore shear instability analyzed with a vortex-force formalism, *J. Geophys. Res.*, *114*, C06021, doi:10.1029/2008JC005135.
Wyatt, A. S., R. J. Lowe, S. Humphries, and A. M. Waite (2010), Particulate nutrient fluxes over a fringing coral reef: Relevant scales of phytoplankton production and mechanisms of supply, *Mar. Ecol. Prog. Ser.*, *405*, 113–130.
Zhang, Z., J. Falter, R. Lowe, G. Ivey, and M. McCulloch (2013), Atmospheric forcing intensifies the effects of regional ocean warming on reef-scale temperature anomalies during a coral bleaching event, *J. Geophys. Res. Oceans*, *118*, 4600–4616, doi:10.1002/jgrc.20338.